Computer-Aided Breast Cancer Detection and Diagnosis of Masses Using Difference of Gaussians and Derivative-Based Feature Saliency

William E. Polakowski, Donald A. Cournoyer, Steven K. Rogers, *Fellow, IEEE*, Martin P. DeSimio,* *Member, IEEE*, Dennis W. Ruck, Jeffrey W. Hoffmeister, *Member, IEEE*, and Richard A. Raines, *Member, IEEE*

***Abstract*—A new model-based vision (MBV) algorithm is developed to find regions of interest (ROI's) corresponding to masses in digitized mammograms and to classify the masses as malignant/benign. The MBV algorithm is comprised of five modules to structurally identify suspicious ROI's, eliminate false positives, and classify the remaining as malignant or benign. The focus of attention module uses a difference of Gaussians (DoG) filter to highlight suspicious regions in the mammogram. The index module uses tests to reduce the number of nonmalignant regions from 8.39 to 2.36 per full breast image. Size, shape, contrast, and Laws texture features are used to develop the prediction module's mass models. Derivative-based feature saliency techniques are used to determine the best features for classification. Nine features are chosen to define the malignant/benign models. The feature extraction module obtains these features from all suspicious ROI's. The matching module classifies the regions using a multilayer perceptron neural network architecture to obtain an overall classification accuracy of 100% for the segmented malignant masses with a false-positive rate of 1.8 per full breast image. This system has a sensitivity of 92% for locating malignant ROI's. The database contains 272 images (12 b, 100μm) with 36 malignant and 53 benign mass images. The results demonstrate that the MBV approach provides a structured order of integrating complex stages into a system for radiologists.**

***Index Terms*— Breast cancer, medical imaging, model-based vision, neural networks.**

I. Introduction

THE National Cancer Institute estimates that annually in the United States over 182 000 women are newly diagnosed with breast cancer, with over 46 000 deaths [1] making it the second leading cause of death from cancer (following lung cancer) for women [2]. Current estimates predict the rate will increase for the foreseeable future [1], [2]. The lifetime risk that a woman will develop breast cancer is one in eight, assuming longevity of 95 years [3].

Although radiologist diagnosis of breast cancer using X-ray film mammograms has allowed for more efficient diagnosis of breast cancers at an earlier stage of development, radiologists misdiagnose 10–30% of the malignant cases; two-thirds of which are retrospectively evident in the mammogram [4]. Of the cases sent for surgical biopsy, only 10–20% are actually malignant [4]. A computer aided diagnosis (CADx) system assisting the radiologist could have a tremendous impact by helping to correctly diagnose the missed malignant cases and reduce the number of unnecessary surgical biopsies.

This work applies a new model-based vision (MBV) paradigm to this CADx area [5]. As applied to medical diagnosis, this MBV architecture consists of five modules. The focus of attention (FOA) module segments suspicious regions in the mammogram, the indexing module separates the regions into size dependent categories and reduces the number of false regions of interest (ROI's), the prediction module develops models for each tissue type in each category, the feature extraction module obtains features from suspicious ROI's, and the matching module classifies the regions. this paradigm breaks the process into key tasks and interfaces them into one integrated algorithm.

The specific application for this MBV algorithm is the detection and classification of mass lesions, lumps of tumorous tissue typically ranging in size from 0.4 cm to greater than 3.0 cm in diameter. Since mass lesions appear very similar to glands, cysts, or dense portions of the breast, and are frequently hidden inside of these regions [6], they can be difficult to distinguish. The spiculation of the mass is usually the dominant feature used for diagnosis, but shape, size, margin, and texture features have also been used [7]–[11].

For computer diagnosis, Kegelmeyer used a local oriented edge analysis algorithm, Laws texture analysis, and a binary decision-tree classification algorithm to detect and classify spiculated lesions [7]. Giger and colleagues used a bilateral subtraction of the opposing mammographic views to detect masses [4], [12], [13]. They relied on histogram and morphological steps to determine the spiculation and margination of the masses for classification.

Our algorithm uses mass size and contrast characteristics for detection, and shape, size, contrast, and Laws texture features for classification. In addition, feature saliency techniques are

Manuscript received December 8, 1995; revised May 1, 1997. The Associate Editor responsible for coordinating the review of this paper and recommending its publication was L. P. Clarke. *Asterisk indicates corresponding author.*

W. E. Polakowski and D. W. Ruck are with the Air Force Information Warfare Center, San Antonio, TX 78243 USA.

D. A. Cournoyer and R. A. Raines are with the Air Force Institute of Technology (AFIT), Wright-Patterson AFB, OH 45433 USA.

S. K. Rogers is with the Cognitive Systems Group, Battelle Memorial Institute, Columbus, OH 43201 USA.

*M. P. DeSimio is with Air Force Institute of Technology (AFIT), Wright-Patterson AFB, OH 45433 USA. He is also with Qualia Computing, Incorporated, Beavercreek, OH 45431 USA (e-mail: martin_desimio@qualia-computing.com).

J. W. Hoffmeister is with Air Force Material Command, Wright-Patterson AFB, OH 45433 USA.

Publisher Item Identifier S 0278-0062(97)09276-8.

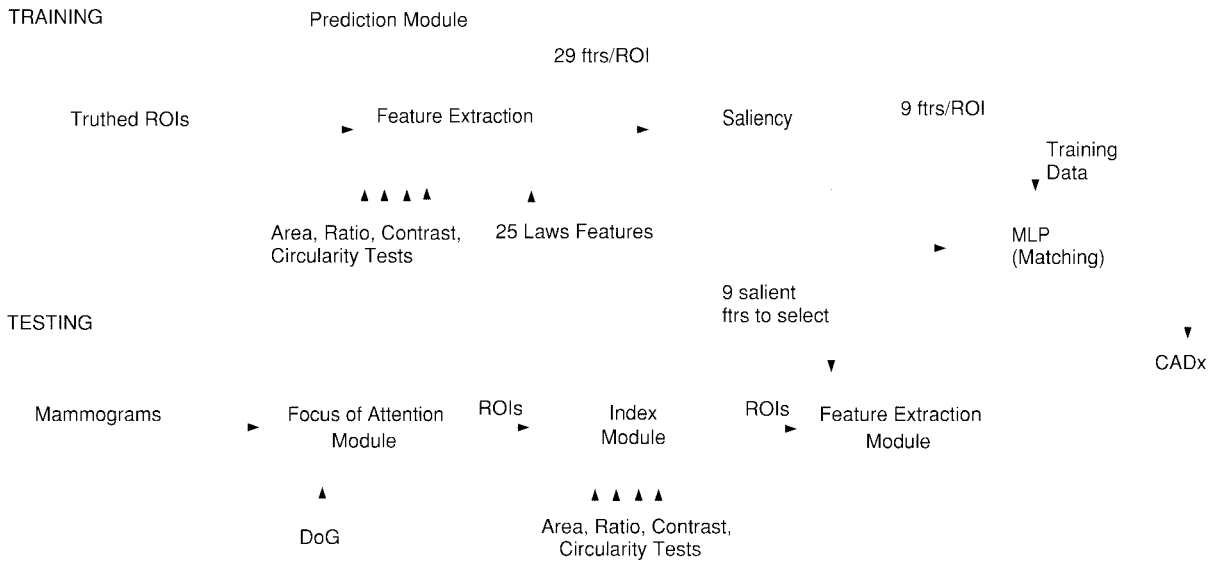

Fig. 1. The model-based vision flow diagram.

used to systematically select the best features [14]–[18].

The following sections present the MBV algorithm and how each module is used. Section II provides a MBV overview followed by a detailed description of each module's function. The database is described in Section III. The results are presented in Section IV, followed by a discussion of the applicability of the MBV approach in mammography.

II. Overview of Model-Based Vision

The MBV method is based on finding many possible targets, paring down false alarms, extracting features from remaining ROI's, and matching these features against those previously extracted from truthed models. The rationale behind using a MBV system is that knowledge is embedded in models and reasoning can be performed to identify targets based on a subset of their characteristics. A MBV system is comprised of modules (Fig. 1). The FOA module is a mechanism for selecting likely targets. The module is designed to get all possible targets. The process will eliminate much of the background. Output of the FOA module is a collection of ROI's surrounding area where one or more targets may be present. The indexing module minimizes the number of ROI's without eliminating the correct target. Feature Extraction provides compact, quantitative descriptions of ROI characteristics. The prediction module extracts information from truthed targets. The matching module determines correspondence between extracted and predicted features to form a classification.

The MBV architecture is used to direct the radiologist's attention to indexed and classified ROI's in a mammogram. The initial FOA module identifies potential ROI's. The indexing module performs tests on the ROI's to reduce the number of false ROI's. From indexed regions, textural features are extracted in the feature extraction module. Using truthed data, the prediction module provides models of benign and malignant tissue. The matching module uses the actual and predicted features from the corresponding modules to achieve a hypothesis. The resulting classification could then be presented to the radiologist.

The modules contain many parameters which have been found to work best for images in our database. The tradeoffs of choosing different values for parameters were analyzed using free-response receiver operating characteristic (FROC) analysis. Through FROC analysis and preliminary experimentation, the best parameter levels were selected for many modules within our algorithm.

A. Focus of Attention Module

The purpose of this module is to separate mass-like regions from the rest of the mammogram. Wavelets have been used to find microcalcifications in mammograms [17], [19], [20]. DoG's have also been successful in microcalcification detection [21]. A similar approach of DoG filtering can be applied to distinguish particular frequency ranges of an image where masses appear.

The DoG filter is constructed by subtracting two Gaussians of different standard deviations and taking the Fourier transform [22]–[24]

$$\frac{1}{2\pi\sigma^2}e^{-(x^2+y^2)/2\sigma^2} \Longleftrightarrow e^{-\sqrt{2\pi}\sigma^2(f_x^2+f_y^2)}. \quad (1)$$

The DoG convolutional kernel and its transfer function are shown in Fig. 2.

To ensure energy normalization, the DoG mask is defined as

$$h(x, y) = \frac{1}{2\pi\sigma_1^2}e^{-(x^2+y^2)/2\sigma_1^2} - \frac{1}{2\pi\sigma_2^2}e^{-(x^2+y^2)/2\sigma_2^2}. \quad (2)$$

Using the Fourier transform, the transfer function becomes

$$H(f_x, f_y) = e^{-\sqrt{2\pi}\sigma_1^2(f_x^2+f_y^2)} - e^{-\sqrt{2\pi}\sigma_2^2(f_x^2+f_y^2)}. \quad (3)$$

The bandpass characteristic of the filter is tuned to the desired frequency by adjusting the standard deviations of the Gaussians to $\sigma_1 = 20$ and $\sigma_2 = 50$. The DoG filter used for our system is matched to masses approximately 1 cm in

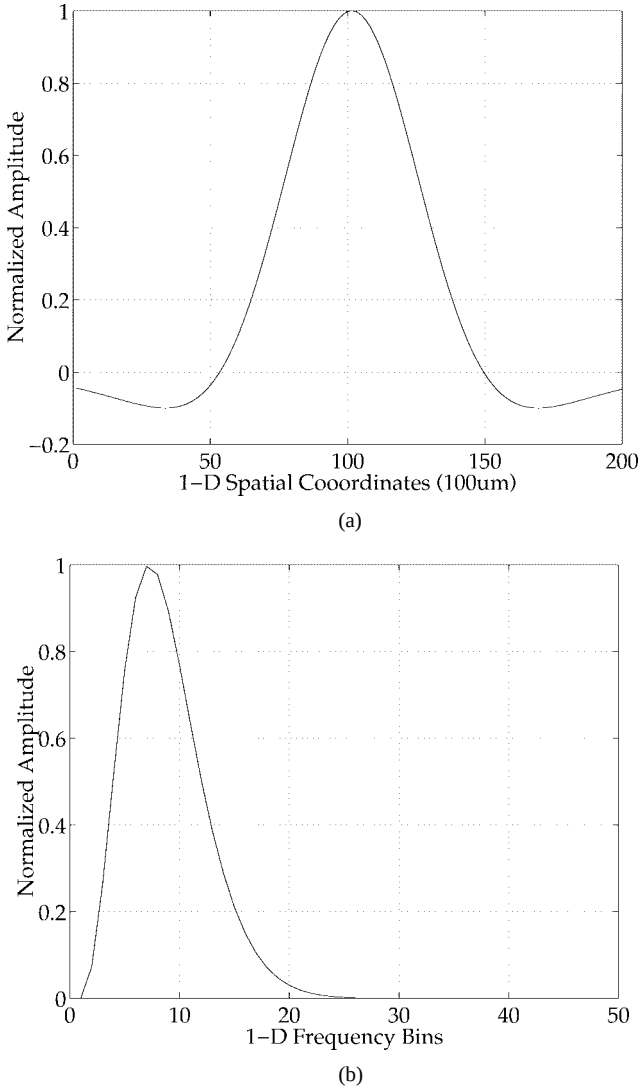

Fig. 2. (a) One-dimensional (1-D) DoG convolutional kernel. The horizontal axis corresponds to 2 cm. (b) One-dimensional DoG transfer function.

diameter. This size is 95 pixels at 100-μm resolution as seen in Fig. 2(a).

First, we segment breast tissue from background by noting that all background pixels in this database had lower gray scale values and thresholding. This value will be database dependent. Extending this method to other databases would not be a problem since breast tissue will have higher intensity levels than the background. Artifacts from wrap-around error will occur with fast Fourier transform-based convolution [25]. A horizontal gradient fill algorithm is implemented to reduce these artifacts. This algorithm finds the difference between the left and right edges of each row of the breast and fills the background with a linear intensity gradient fill. The results of the horizontal fill are shown in Fig. 4(a) for the image of Fig. 3(a). The top-to-bottom convolution artifacts are removed by truncating the erroneous section at the top of the mammogram as shown in Fig. 4(b). This truncation may remove a small portion of breast tissue, but this area has a lower probability of containing a mass and for this database contains no masses. Upon implementation of the DoG on this

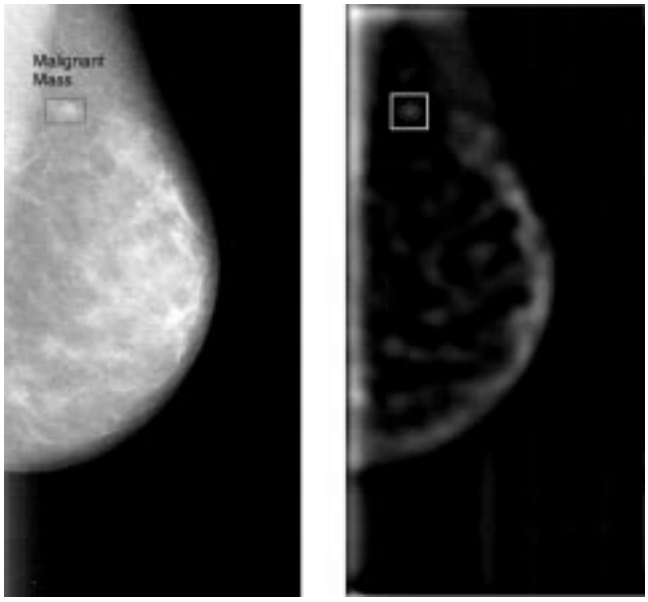

Fig. 3. (a) Mammogram with a radiologist-truthed malignant mass in box and (b) DoG filter results on the original image.

preprocessed image, the interior structure of the breast and, thus, the mass is much more visible [Fig. 4(b)]. By setting a global threshold of the maximum gray scale in the processed image, distinct mass-like regions are found [Fig. 4(c)] and sent to the index module for the next step in the MBV process. Optimization of these thresholds are used for a given training database.

B. Index Module

Using the binary image from the FOA module and the original gray-scale image, the indexing module labels each grouping of pixels. A discrete set of size-dependent categories are passed on and subjected to a set of tests to reduce the number of false ROI's.

The masses for this research are categorized into four sizes: small (diameter less than 0.5 cm), medium (between 0.5 cm and 2.0 cm), large (between 2.0 and 4.0 cm), and extra large (greater than 4.0 cm). This research is focused on finding medium-sized masses. Large masses are also found and classified, but extra large and small masses were not addressed. Larger masses are those most likely palpable and are less difficult for radiologist to find on mammograms. Medium masses are chosen for this study since all but three masses in the database fell in this category.

After subjecting each region to a bounding-box to perimeter criterion, the regions are indexed as medium or large ROI's. The bounding-box to perimeter criterion is defined as the ratio of the area of the smallest box containing the entire detection to the number of pixels forming its perimeter.

Since there are only two Large ROI malignant masses in the database, and since large (palpable) masses are in general more easily diagnosed, no further processing is done on the indexed Large ROI's. Thus, all false large ROI's are treated as false-positives.

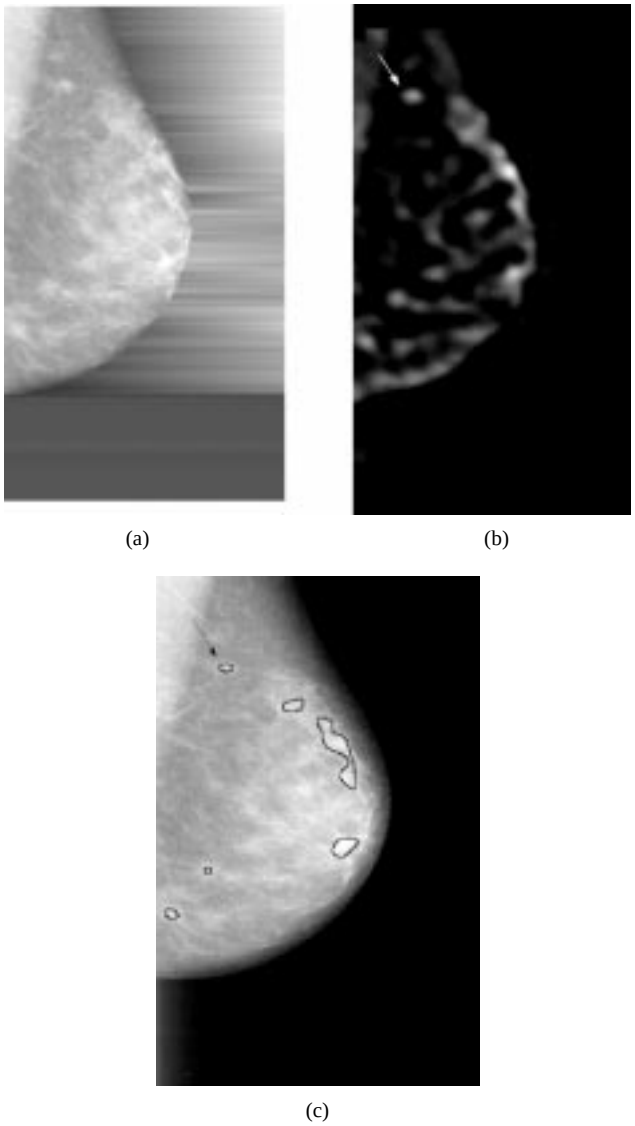

Fig. 4. (a) Image gradient fill results applied to the image shown in Fig. 3(a), (b) DoG filter results on the processed image, and (c) binary overlay identifying mass-like regions in the processed image. The true malignant mass is identified by the arrow.

All further processing is done on the medium ROI's, 140×140 pixel regions centered on the centroid of the detected mass. The ROI's are sorted by their bounding-box to perimeter ratio. Since the malignant regions all have relatively high ratios, only the top seven (of up to 22) ROI's per image are retained. Then, a mask containing the top 15% of the ROI gray scale is created for each ROI [Fig. 5(b)]. For ROI's containing mass-like tissue, these top 15% of the pixels are contained within the mass region, while for normal tissue, the pixels are scattered throughout the ROI. Morphological processes are implemented to eliminate nonmass-like ROI's. The histogram mask is first eroded [Fig. 5(c)]. To eliminate spurious small pixel clusters, groups of pixels smaller than 1000 pixels are eliminated. Using 100-μm film, 1000 pixels translates to a circular mass with a diameter of less than 4 mm, which are not considered in this work. Finally, the mask is dilated and closed to obtain a solid, well-defined mask shape [Fig. 5(d)].

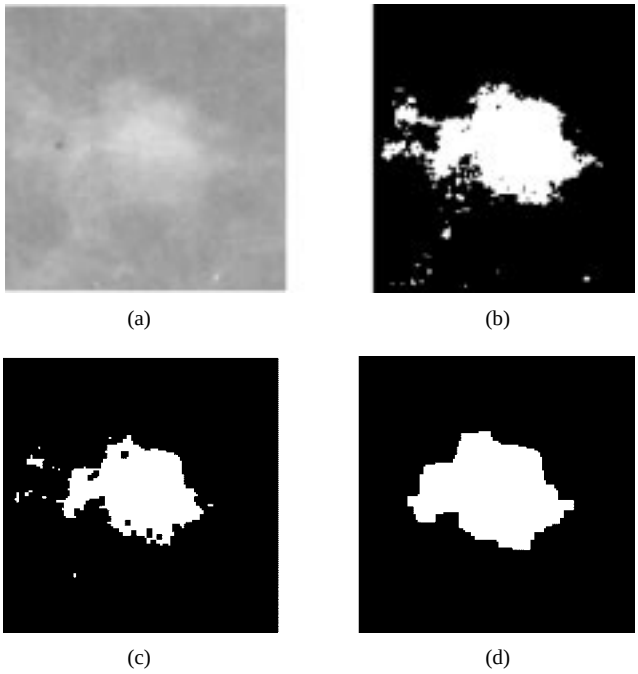

Fig. 5. The ROI from Fig. 3(a) and its morphological masks: (a) malignant mass ROI, (b) top 15% of the gray scale intensity, (c) erosion, and (d) final mask.

The ROI's surviving the above steps are subjected to another area test (area $>$ 1000 pixels), a contrast test (contrast $>$ 0.02), and a circularity test (circularity $>$ 0.58) [13]. The area test eliminates any ROI's containing less than 1000 pixels, since some areas became disjoint through the morphological operations. Many false ROI's are eliminated by this method since the thresholding gives smaller regions spread evenly throughout the ROI, disjoint of a mass-size object. The contrast test obtains the ratio of the average value in the gray scale ROI [Fig. 5(a)] covered by the mask [Fig. 5(d)] minus the rest of the ROI's average gray scale to the sum of the averages [26]. Thus, with a contrast of 0.02, the area under the mask is only slightly brighter than the surrounding area. The circularity test constructs a circle with area equal to the mask's area. Centering the circle over the centroid of the mask, the circularity is the fraction of the overlapping areas. The tests are cascaded to perform further tests only on the surviving ROI's. Finally, only up to the four most circular regions are retained per image. On average, only two ROI's are specified per image, but at most, a radiologist would be directed to the four most mass-like regions in a mammogram.

C. Prediction Module

The purpose of the prediction module is to define models of malignant and nonmalignant mass tissue. Many researchers have used Laws texture features [7], [11], [27], to classify malignant masses, but none have used any objective criterion to determine which Laws kernels work best. This work identifies the best kernels for finding malignant mass tissue through feature saliency techniques. Saliency refers to the discrimination information or power of a feature.

Twenty-five 5×5 Laws convolutional kernels are derived from all possible matrix multiplications of the five vectors

TABLE I
LAW'S 1-D KERNELS

Kernel Name	Kernel Label	Kernel Values
Average	l	(1 4 6 4 1)
Spot	s	(−1 0 2 0 −1)
Edge	e	(1 −4 6 −4 1)
Ripple	r	(−1 −2 0 2 1)
Wave	w	(−1 2 0 −2 1)

TABLE II
THE TOP NINE FEATURE RANKINGS

Derivative Rank	Feature
1	w5r5 kernel
2	r5r5 kernel
3	s5s5 kernel
4	s5e5 kernel
5	e5s5 kernel
6	l5s5 kernel
7	e5w5 kernel
8	l5e5 kernel
9	area

Fig. 6. MLP classifier architecture using inputs as listed in Table II.

shown in Table I. The 25 Laws features [28] are found by summing the absolute value of all pixels within the binary mask of the result of the convolution of the 5×5 kernel with the gray-scale ROI. Using statistical and derivative-based feature saliency techniques, the best of these features combined with those derived from the ratio, area, contrast, and circularity tests, are chosen, obtaining up to the best ten features out of the 29 available.

The reason for the reduction in features is that good generalization requires that the minimum number of training samples in a class must be at least three times the number of features [29], [30]. With 36 malignant samples available for training and testing, the number of features should be less than twelve.

The derivative-based saliency technique uses the derivative at each output node of a trained neural network classifier with respect to the input features [14]–[18]. The neural network is a single perceptron, having 29 inputs and one output.

The derivative-based neural network feature saliency algorithm is used to select the features that have the biggest effect on determining the neural network classifier's decision boundary. However, since the number of nonmalignant ROI's outnumbered the number of malignant ROI's by a factor of almost three to one, an imbalanced training set neural network weight update algorithm ensures the network trained to the minimum mean-squared error for both classes instead of only for the dominant class [31]. With this final modification, ten feature saliency trials are run. Since seven features appeared in the top ten in all ten trials and two others in six trials, those nine features are used to develop the malignant/nonmalignant model (Table II). The resultant multilayer perceptron (MLP) classifier architecture is shown in Fig. 6.

D. Feature Extraction

The purpose of the feature extraction module is to obtain the information specified from feature saliency from the ROI's passed from the index module. Once the ROI's are passed from the index module, the feature extraction module gets from the ROI's the nine features specified by the prediction module. The feature vectors are then input to the matching module for classification.

E. Matching Module

The matching module uses the features as selected from the feature extraction and prediction modules. A MLP is trained from the features of the prediction module. When wanting to diagnose ROI's, the features are obtained from the extraction module and input into the MLP. The result is a classification of malignant or benign tissue.

III. DATABASE

The Lumiscan 200 automatic laser film digitizer (Lumisys, Sunnyvale, CA) was used to digitize the mammograms at 100-μm resolution with 12-b grayscale. Each full breast image varied from 1500 to 1800 columns by 2400 to 2500 rows. To make the database uniform and manageable, the breast areas were extracted from the images resulting in a 1024×2048 array. In most cases, no tissue shown on the X-ray film was lost; if tissue had to be cropped, it was taken from the chest wall side of the image.

The database was split into four categories of images: 1) malignant mass training (ten cases totaling 18 images); 2) malignant mass testing (nine cases, 18 images); 3) benign mass testing (28 cases, 53 images); 4) nonmass testing (183 images). the malignant mass training and testing sets each contained exactly one biopsy-proven malignant mass per image. The training set was used to define and develop the algorithm. The testing set was used to evaluate and modify the algorithm. The benign mass set consisted of biopsy-truthed masses diagnosed benign. The benign set tested the algorithm's ability to reduce the number of unnecessary biopsies. The size distribution of masses for these three data sets is shown in Fig. 7. The contrast, defined as the ratio of the difference of the averages inside and outside approximately equal areas of the mass to the sum of the averages [26], was found for all ROI's (Fig. 8). The images in the nonmass set either contained benign microcalcifications, malignant microcalcifications, or were one of the other mammographic views of a breast that had not been biopsied.

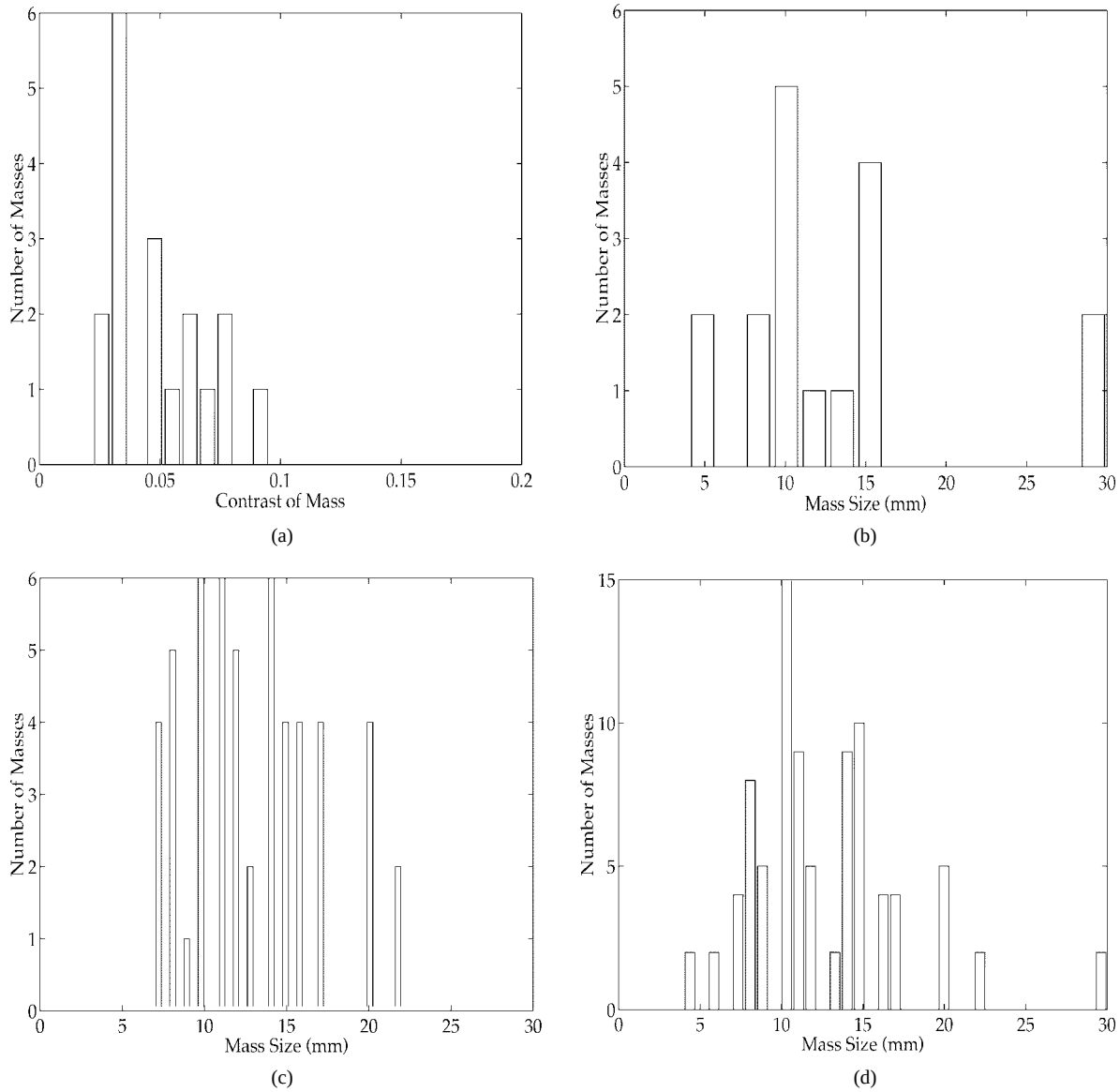

Fig. 7. Mass sizes for (a) malignant mass training set, (b) malignant mass testing set, (c) benign mass set, and (d) total of mass database. Note: scale on (d) is different than others.

The mammograms selected for this research were not hand picked to provide the best results. The malignant cases were consecutive cases with malignant pathology from 1991 to 1995. The benign cases were chosen by selecting the benign case closest in time to each malignant case. Therefore, the database consisted of a balanced dataset with approximately the same number of benign and malignant cases. As many cases as possible were selected for this study to ensure a good cross section of typical mass cases.

IV. Results

The focus of this research was to provide a model-based vision tool to assist radiologists by computer detection of masses in mammograms. During algorithm development, tradeoffs were made between 1) the number of true detections obtainable at the expense of having more false detections and 2) diagnosing correctly all malignant regions while misdiagnosing some benign regions. Modules have parameters which affect performance. The interaction of tradeoffs and parameters is best observed in FROC curves. FROC analysis determined the operating points for the algorithm. These plots give a complete view of the performance of the algorithm in terms of true-malignant, false-malignant, true-benign, and false-benign information. Similar FROC analysis has been used previously in radiology [4], [32].

Since the MBV system is composed of stages, analysis needs to be performed on each module to eliminate false positives without removing the true mass detection. The FOA module is the first screening, so it is important not to eliminate true ROI's. We accept a high false-alarms rate to be reduced later. While holding constant parameters, such as the DoG size, analysis was performed on the effect of passing different numbers of the largest ROI's to the indexing module. The final operating point was chosen to retain the seven largest medium-size ROI's. For the training and testing data, this produced 92% correct segmentation of malignant regions (18 out of 18

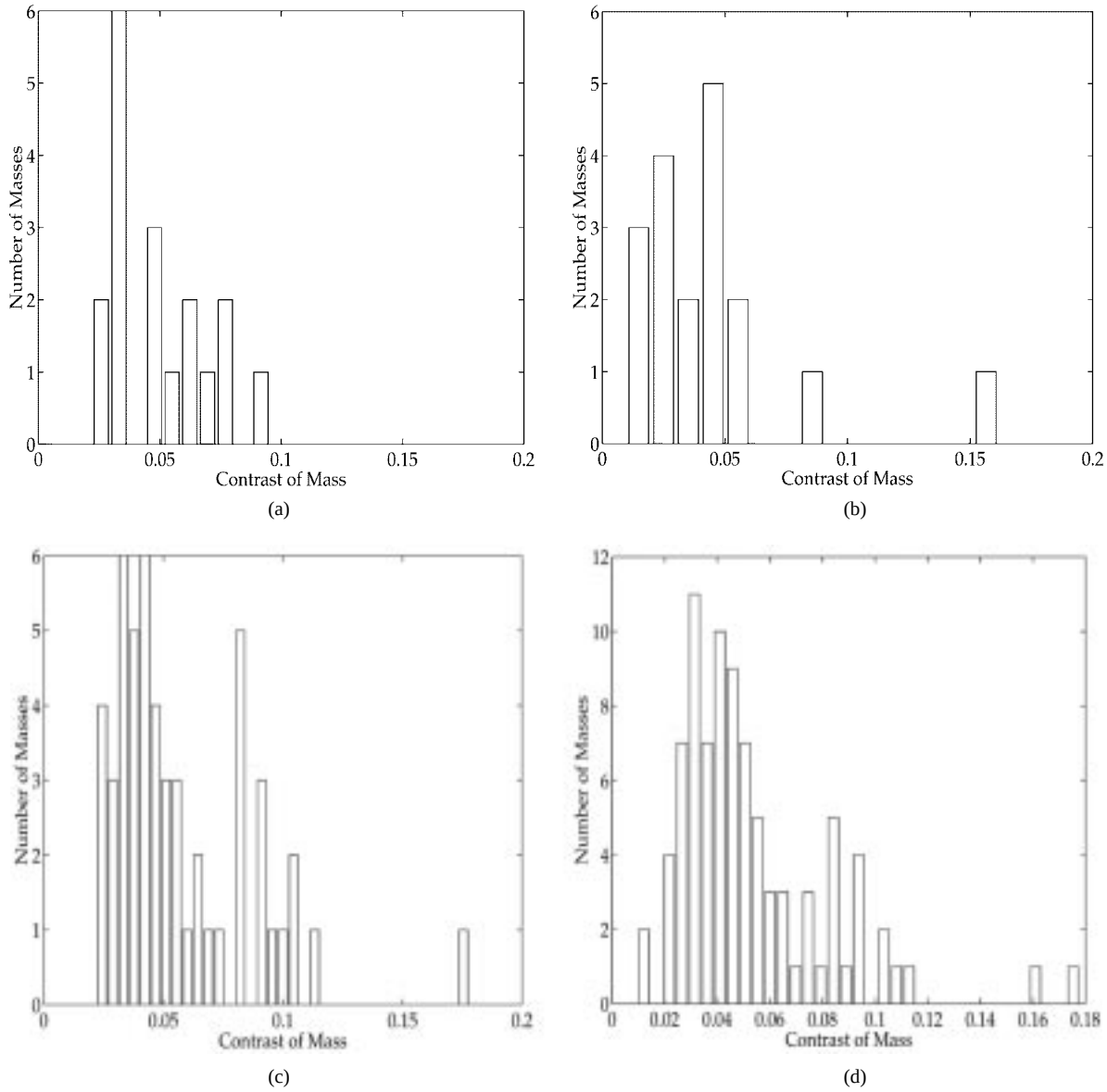

Fig. 8. Contrast for (a) malignant mass training set, (b) malignant mass testing set, (c) benign mass set, and (d) total of mass database, note: scale on (d) is different than others.

during training and 15 of 18 during testing) and an average of five false ROI's per image being passed on to the index module.

The FROC analysis for the indexing module (shown in Fig. 9) was performed in a similar manner. However, the goal of this module was to decrease the number of false ROI's. The number of top circular ROI's to be passed to the prediction module was chosen to be four, thus, allowing for the algorithm to remain at 92% detection while decreasing the number of false ROI's from 8.39 to 2.36 per image (see Table III).

The prediction module extracted the 25 Laws features and used them in conjunction with the index module's four features to determine the best ones to use to develop the malignant mass and nonmalignant tissue models. By training on 33 malignant ROI's, 39 benign-biopsied ROI's, and 45 other false ROI's, nine features appeared in the top ten rankings in over half of the ten feature saliency trials. It is interesting to note, that the four kernels Kegelmeyer selected as being the best (l5s5, l5e5, r5r5, and e5s5) [7], also appeared in the top nine derivative-based saliency features; thus, providing a formal means of confirming their utility.

The matching module used the nine features found from the prediction module and determined the best neural network architecture and weights to use for the classification of all the medium ROI samples. Of the ten trials, the weights for the best trial were chosen as the best model/classification architecture combination. A tradeoff was made to classify all malignant samples at the expense of misdiagnosing a benign tumor as malignant. These weights correctly classified all 33 malignant samples as malignant for a true-positive rate of 1.0. The same weights correctly classify 270 of the 643 benign samples as benign, for a false-positive rate of 0.58. Of those false-positives, only 15 of the 53 radiologist highlighted benign-biopsied masses were misclassified as malignant. Fig. 10 shows an example final output to the radiologist with the computer's diagnosis. The computer diagnosed correctly the malignant

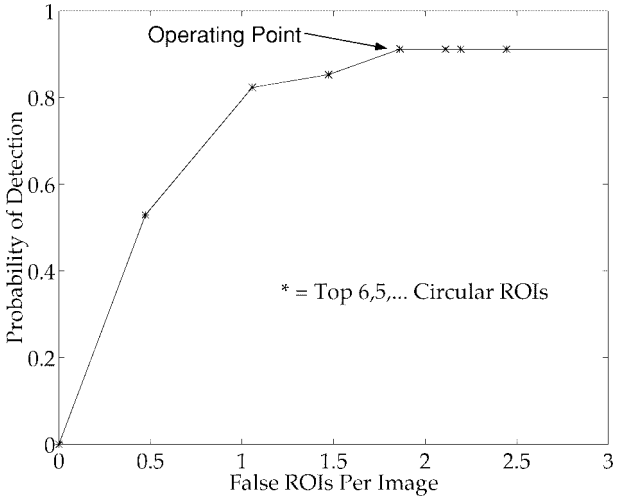

Fig. 9. FROC Curve for the index module.

TABLE III
RESULTS FOR THE FOA MODULE, INDEX MODULE, MATCHING MODULE, AND COMPLETE SYSTEM ON 272 IMAGES. THE TOTAL ROI COUNT FOR THE MATCHING MODULE AND FINAL RESULTS INCLUDE 270 CORRECTLY DIAGNOSED BENIGN ROI'S. TP AND FP REFER TO THE TP FRACTION AND FP FRACTION, RESPECTIVELY. THE /img IS THE NUMBER OF OTHER ROI'S PER IMAGE AT EACH STAGE

Data Set	Total ROI's	Malignant		Other ROI's		
		ROI's	TP	ROI's	/img	FP
FOA	2314	33/36	0.92	2281	8.39	NA
Index	676	33/33	1.0	643	2.36	NA
Matching	676	33/33	1.0	373	1.8	0.58
Final	676	33/36	0.92	373	1.8	0.58

mass and two of the three benign regions, one benign region was misdiagnosed as malignant. Thus, there was one false alarm, and three correct diagnoses for this image.

V. DISCUSSION

This MBV approach to mass detection is useful as a second opinion to a radiologist. The FOA module's DoG filter in conjunction with the indexing module's morphological operations and tests proved to be an effective tool for locating malignant ROI's in mammograms. The MBV algorithm detected 92% of the malignant ROI's with less than two false malignant ROI's per image. The prediction module, through feature saliency, selected the best nine features. Classification results using these nine features provide a true-positive fraction of 1.0 and a false-positive fraction of 0.58. By designing the prediction and matching modules with all of the data rather than just the training set, these results may be optimistically biased. However, due to the small number of malignant samples, all were used to train the MLP classifier and subsequently tested. In future work as a larger database becomes available, design will be based on training data alone, thus eliminating the possible bias.

This work was dependent on setting many parameters in each module. The parameters are characteristic for this database of images, since they are dependent on specific

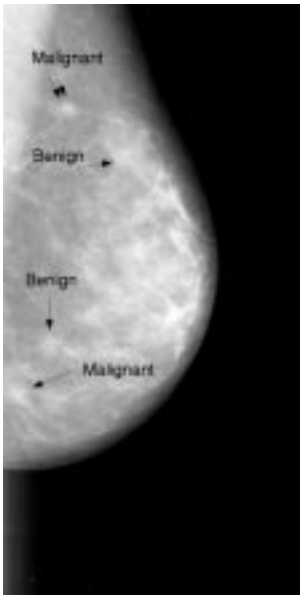

Fig. 10. The final output to the radiologist showing the original example image with the suspicious regions and the computer's classification identified. The true malignant mass is identified by the double arrow. The other three regions are truly benign regions.

items, such as the film, X-ray machine, and digitizer. These parameters were obtained through preliminary experimentation and FROC analysis using the training images. Extending this algorithm to another database would be tedious, but not difficult. By using a genetic algorithm, the database-dependent parameters could be found for any particular database. The DoG parameters, the standard deviations chosen for the DoG, can be varied dependent on the size of the object being evaluated, thus, making DoG filtering extensible to microcalcification detection [21].

The model-based vision approach is well suited to CADx of mammograms and to the process of radiologists. This approach uses a structured means of generous ROI selection followed by reduction of irrelevant ROI's. This process allows for a coupling of engineering technology with medical practices in a block-by-block approach, allowing for adjustments to the algorithm box-by-box in order to adapt parameters to the radiologists preferences. This control allows the radiologist to set conservative thresholds for finding all malignant masses. A CADx system has a future in mammography as a second opinion to radiologists. The MBV vision algorithm has shown it can contribute to the CADx process.

REFERENCES

[1] J. H. Tanne, "Everything you need to know about breast cancer...but were afraid to ask," *New York [GNYC]*, vol. 26, pp. 52–62, Oct. 1993.
[2] R. A. Smith, "Epidemiology of breast cancer," *RSNA Categorical Course Phys.*, pp. 21–33, 1994.
[3] "Breast cancer: New perspectives can replace unrealistic fears," Mayo Foundation for Medical Education and Research, Rochester, MN, Tech. Rep. ISSN 0741-6254, Oct. 1994.
[4] M. L. Giger, "Computer-aided diagnosis," *RSNA Categorical Course Phys.*, pp. 283–298, 1993.
[5] E. Zelnio, "ATR legacy," presented at *MSTAR Program Initiation Meeting*, Wright Laboratory, Wright-Patterson AFB OH, Sept. 1995.
[6] E. S. de Paredas, "Radiographic breast anatomy: Radiologic signs of breast cancer," *RSNA Categorical Course Phys.*, pp. 35–46, 1994.

[7] W. Kegelmeyer, J. M. Pruneda, P. D. Bourland, A. Hillis, M. W. Riggs, and M. L. Nipper, "Computer-aided mammographic screening for spiculated lesions,"*Radiol.,* vol. 191, pp. 331–337, May 1994.
[8] Y. Wu, M. Giger, K. Doi, C. Metz, C. Vyborny, and R. Schmidt, "Artificial neural networks in mammography: Application to decision making in the diagnosis of breast cancer,"*Radiol.,* vol. 187, pp. 955–963, Sept. 1993.
[9] P. Miller and S. Astley, "Classification of breast tissue by texture analysis,"*Image Vision Comput.,* vol. 10, no. 5, pp. 277–281, 1992.
[10] S. M. Lai, X. Li, and W. Bischof, "On techniques for detecting circumscribed masses in mammograms," *IEEE Trans. Med. Imag.,* vol. 8, pp. 377–386, Dec. 1989.
[11] D. Wei, H. P. Chan, M. A. Helvie, B. Sahiner, N. Petrick, D. D. Adler, and M. M. Goodsitt, "Classification of mass and normal breast tissue on digital mammograms: Multiresolution texture analysis," *Med. Phys.,* May 1995.
[12] M. L. Giger, F.-F. Yin, K. Doi, C. E. Metz, R. A. Schmidt, and C. J. Vyborny, "Investigation of methods for the computerized detection and analysis of mammographic masses," *SPIE,* vol. 1233, pp. 183–184, 1990.
[13] F.-F. Yin, M. L. Giger, K. Doi, R. A. Schmidt, and C. J. Vyborny, "Computerized detection of masses in digital mammograms: Investigation of feature analysis techniques," *J. Digital Imag.,* vol. 7, no. 1, pp. 18–26, 1994.
[14] D. W. Ruck, S. K. Rogers, and M. Kabrisky, "Feature selection using a multi layer perceptron," *J. Neural Network Comput.,* vol. 2, pp. 40–48, Oct. 1990.
[15] D. W. Ruck and S. K. Rogers, *Feature Selection for Pattern Recognition Using Neural Networks*, Industry Electronics Handbook. Boca Raton, FL: CRC, June 1995.
[16] J. M. Steppe, K. W. Bauer, S. K. Rogers, "Integrated Feature and architecture selection," *IEEE Trans. Neural Networks,* vol. 7, pp. 1007–1014, 1996.
[17] C. M. Kocur, S. K. Rogers, L. R. Myers, T. Burns, M. Kabrisky, J. W. Hoffmeister, K. W. Bauer, and J. M. Steppe, "Using neural networks to select wavelet features for breast cancer diagnosis," *IEEE Eng. Med., Biol., Mag.,* May 1996.
[18] R. C. Dauk, S. K. Rogers, D. W. Ruck, J. W. Hoffmeister, and R. A. Raines, "A comparative study of texture measures for the classification of breast tissue," *IEEE Trans. Syst., Man, Cybern.,* submitted for publication.
[19] D. McCandless, S. K. Rogers, J. W. Hoffmeister, D. W. Ruck, R. A. Raines, and B. W. Suter, "Model based detection of clustered microcalcifications using wavelets and phantom derived features," *IEEE Trans. Med. Imag.,* submitted for publication.
[20] H. Yoshida, K. Doi, and R. M. Nishikawa, "Automated Detection of clustered micro calcifications in digital mammograms using wavelet transform techniques," *SPIE Image Processing,* vol. 2167, pp. 868–886, 1994.
[21] E. Ochoa, T. Rathbun, J. Hoffmeister, S. Rogers, and M. DeSimio, "Automated clustered microcalcification detection using optimized difference of Gaussians," *IEEE Trans. Med. Imag.,* submitted for publication.
[22] B. Jahne, *Digital Image Processing Concepts, Algorithms and Scientific Applications.* New York: Springer-Verlag, 1991.
[23] D. Marr, *Vision.* San Francisco: Freeman, 1982.
[24] J. D. Gaskill, *Linear Systems, Fourier Transforms, and Optics.* New York: Wiley, 1978.
[25] R. C. Gonzalez and R. E. Woods, *Digital Image Processing.* Reading, MA: Addison-Wesley, 1992.
[26] W. Morrow, R. Paranjape, R. Rangayyan, and J. Desautels, "Region-based contrast enhancement of mammograms," *IEEE Trans. Med. Imag.,* vol. 11, no. 3, pp. 392–406, Sept. 1992.
[27] P. Miller and S. Astley, "Classification of breast tissue by texture analysis," *Image Vision Comput.,* vol. 10, pp. 277–282, June 1992.
[28] K. I. Laws, "Textured image segmentation," *Image Processing Institute, Univ. Southern California,* vol. 940, Jan. 1980.
[29] S. K. Rogers and M. Kabrisky, *An Introduction to Biological and Artificial Neural Networks for Pattern Recognition.* Bellingham, WA: SPIE Optical Eng. Press, 1991.
[30] D. H. Foley, "Considerations of sample and feature size," *IEEE Trans. Inform. Theory,* vol. IT-18, pp. 618–626, Sept. 1972.
[31] R. Anand, K. G. Mehrotta, C. K. Mohan, and S. Ranka, "An improved algorithm for neural network classification of imbalanced training sets,"*IEEE Trans. Neural Networks,* vol. 4, pp. 962–969, Nov. 1993.
[32] C. E. Metz, "ROC methodology in radiologic imaging," *Investigat. Radiol.,* vol. 21, pp. 720–733, Sept. 1986.